PCCP

Cite this: *Phys. Chem. Chem. Phys.*, 2011, **13**, 17615–17624

www.rsc.org/pccp

**PAPER**

# Graphene and carbon nanotube composite electrodes for supercapacitors with ultra-high energy density

**Qian Cheng,[ab] Jie Tang,*[ab] Jun Ma,[a] Han Zhang,[a] Norio Shinya[a] and Lu-Chang Qin[c]**

***Received 12th June 2011, Accepted 10th August 2011***
**DOI: 10.1039/c1cp21910c**



We describe a graphene and single-walled carbon nanotube (SWCNT) composite film prepared by a blending process for use as electrodes in high energy density supercapacitors. Specific capacitances of 290.6 F $g^{-1}$ and 201.0 F $g^{-1}$ have been obtained for a single electrode in aqueous and organic electrolytes, respectively, using a more practical two-electrode testing system. In the organic electrolyte the energy density reached 62.8 Wh $kg^{-1}$ and the power density reached 58.5 kW $kg^{-1}$. The addition of single-walled carbon nanotubes raised the energy density by 23% and power density by 31% more than the graphene electrodes. The graphene/CNT electrodes exhibited an ultra-high energy density of 155.6 Wh $kg^{-1}$ in ionic liquid at room temperature. In addition, the specific capacitance increased by 29% after 1000 cycles in ionic liquid, indicating their excellent cyclicity. The SWCNTs acted as a conductive additive, spacer, and binder in the graphene/CNT supercapacitors. This work suggests that our graphene/CNT supercapacitors can be comparable to NiMH batteries in performance and are promising for applications in hybrid vehicles and electric vehicles.

## Introduction

With a fast-growing market for portable electronic devices and the development of hybrid electric vehicles, there has been an ever increasing and urgent demand for energy storage devices that are of high energy density and high power density. While Li-ion batteries have very good energy performance, their power performance is insufficient for many power demanding applications. Supercapacitors, which are also called electrochemical capacitors or ultracapacitors, have attracted much attention in recent years because of their pulse power supply, long cyclic life (> 100 000 cycles), simple operational mechanism, and high dynamics of charge propagation.[1] Supercapacitors have a high power capability and relatively large energy density compared to the conventional capacitors, which have already enabled supercapacitors to be applied in a variety of energy storage systems. For example, they are already used in memory back-up systems, consumer electronics, industrial power supplies, and energy management.[2] A more recent application is the use of supercapacitors in emergency doors on Airbus A380, highlighting their safe and reliable performance.[1] In such cases, supercapacitors are coupled with primary high energy batteries or fuel cells to serve as a temporary energy storage device with a high-power capability. Supercapacitors are likely to show an equal importance as batteries for future energy storage systems.

Carbon-based materials, including activated carbon,[3,4] carbon nanotubes (CNTs),[5,6] and graphene,[7–13] have been widely used in electrochemical double-layer supercapacitors owing to their excellent physical and chemical properties. Activated carbon is the most used electrode material for supercapacitors due to its large surface area and low cost. However, in activated carbon there are a lot of carbon atoms that cannot be accessed by the electrolyte ions as illustrated in Fig. 1a. These carbon atoms are all wasted practically in terms of activating their electrochemical functions. This is a major factor that limits the specific capacitance of activated carbon electrodes. Moreover, the low electrical conductivity of activated carbon is also limiting its applications in high power density supercapacitors and results in a low specific capacitance per area. A higher electrical conductivity and enhanced charge transfer channels of CNTs make them a most promising candidate for energy saving applications. CNTs have now often been regarded as the choice of high-power electrode material because of their improved electrical conductivity and high readily accessible surface area. As illustrated in Fig. 1b, single walled carbon nanotubes (SWCNTs) are very likely to stack in bundles. As a result, only the outermost portion of CNTs can function for ion absorption and the inner carbon

[a] *National Institute for Materials Science, 1-2-1 Sengen, Tsukuba 305-0047, Japan. E-mail: tang.jie@nims.go.jp*
[b] *Doctoral Program in Materials Science and Engineering, University of Tsukuba, 1-1-1 Tennodai, Tsukuba 305-8577, Japan. E-mail: cheng.qian@nims.go.jp*
[c] *Department of Physics and Astronomy, University of North Carolina at Chapel Hill, Chapel Hill, NC 27599-3255, USA. E-mail: lcqin@email.unc.edu*

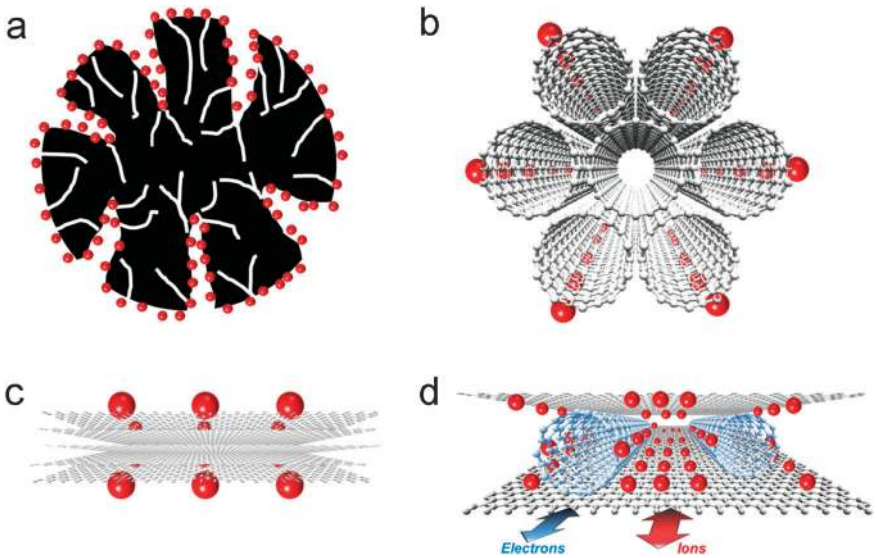


**Fig. 1** Comparison of different carbon materials as electrodes of supercapacitors. (a) Activated carbon. Activated carbon has a high surface area. However, many of the micropores cannot be accessed by electrolyte ions. (b) Single-walled carbon nanotube (SWCNT) bundles. SWCNTs usually form bundles, limiting their surface area. Only the outmost surface can be accessed by electrolyte ions. (c) Pristine graphene. Graphene nano-sheets are likely to agglomerate through van der Waals interactions during the drying process. It would be difficult for electrolyte ions to access the ultra-small pores, especially for larger ions such as an organic electrolyte or at a high charging rate. (d) Graphene/CNT composite. SWCNTs can serve as a spacer between the graphene nano-sheets to give rise to rapid diffusion pathways for the electrolyte ions. Moreover, they can enhance electrical conduction for the electrons. The CNTs also serve as a binder to hold the graphene nano-sheets together preventing disintegration of the graphene structure into the electrolyte.

atoms are all wasted, leading to lower specific capacitance of CNT-based supercapacitors.

On the other hand, graphene, the parent of all graphitic structures, offers an attractive alternative.[14] Graphene is distinctly different from CNTs and fullerenes. Graphene and chemically modified graphene sheets possess a high electrical conductivity,[15] high surface area, and outstanding mechanical properties comparable with or even better than CNTs.[16] The specific surface area of a single graphene sheet is 2630 $m^2 g^{-1}$, which is much larger than that of activated carbon and carbon nanotubes that are usually used in the electrochemical double layer capacitors.[8] These factors make graphene a most promising material for supercapacitors. In a double-layer capacitor there exists a diffuse layer in the electrolyte due to accumulation of ions close to the electrode surface and the double-layer capacitance is between 5 to 20 μF $cm^{-2}$ depending on the electrolyte used.[17] The specific capacitance achieved with aqueous alkaline or acid solutions is usually higher than that with organic electrolytes. The theoretical specific capacitance is 526 F $g^{-1}$ at most in an aqueous electrolyte. Graphene-based materials can be easily obtained by simple chemical processing of graphite.[18] Moreover, a graphene-based structure of individual sheets does not depend on the distribution of pores in the solid support to provide its large surface area. Instead, every chemically modified graphene sheet can "move" physically to adjust to different types of electrolytes. As a result, the access to a very large surface area in graphene-based materials by the electrolyte can be maintained while preserving the overall high electrical conductivity in the network. There have been several recent studies on the potential of graphene as a supercapacitor electrode material. High specific capacitances of 135 F $g^{-1}$ and 205 F $g^{-1}$ have been reported.[8,19,20] However, there are also issues with the pristine graphene-based supercapacitors. Firstly, the chemically reduced graphene usually has an electrical conductivity of about 100–200 S $m^{-1}$, which is two orders of magnitude lower than conductive single-walled carbon nanotubes (usually 10 000 S $m^{-1}$). Secondly, like most nanomaterials, graphene is also likely to form irreversible agglomerates or to restack to form graphite through the van der Waals interactions during the drying process applied in obtaining graphene.[21] In such a case, it would be difficult for the ions to gain access to the inner layers to form electrochemical double layers if the graphene sheets are stacked together. In this case, the ions could only accumulate on the top and the bottom surfaces of the graphene sheets and would then lead to a lower specific capacitance since the stacked material cannot be fully used, as illustrated schematically in Fig. 1c. Thirdly, a graphene electrode cannot function without a binder, which would usually reduce the specific capacitance.

In this work, we describe the use of graphene/CNT composite as the electrode material for electrochemical double layer supercapacitors as shown schematically in Fig. 1d. Graphene has the largest theoretical electrochemical double layer capacitance of about 526 F $g^{-1}$. However, reported experiments could only attain 25.7% to 39.0% of its theoretical value.[8,19,20] A major problem is the re-stacking of graphene sheets. Ions, especially larger organic ions, may have difficulty in accessing the electrode. One solution to overcome the re-stacking of graphene is the proposal of making use of curved graphene.[22] However, according to our experiment, curved graphene sheets also have re-stacking problems which will lower the final specific capacitance of the electrodes. Moreover, to make uniform large curved graphene sheets is difficult. Another idea is to use a spacer instead to change the

 

structure of graphene electrodes. For an electrochemical double layer supercapacitor, we need the spacer to be of high conductivity, high surface area, and have superb mechanical properties. Single-walled carbon nanotubes are an excellent candidate. Single-walled carbon nanotubes have a very high electrical conductivity of 10 000 S $m^{-1}$ which is two orders of magnitude larger than chemically reduced graphene nano-sheets. Therefore the use of CNTs can reduce the internal electrical resistance of the electrode and improve the power performance. The SWCNTs can also function as a smart "spacer" for graphene nano-sheets to prevent agglomeration between each other and therefore to improve the accessibility for electrolyte ions. The electrodes would be accessed more easily by the electrolyte ions with the assistance of spacers and therefore more material could be used electrochemically, which can be seen in Fig. 1d. In addition, the CNTs have excellent binding properties to serve as a binder to hold the graphene nano-sheets together. Recently, attempts have been made to fabricate graphene nano-sheets with CNT films using layer-by-layer and chemical vapour deposition (CVD) techniques for supercapacitors. However, these methods are time consuming and not suitable for large-scale production.[23,24] A hybrid film has also been studied using low temperature solution processing of two carbon-based nanomaterials for transparent conductors, but the ultra-thin film has limited significance for applications in batteries or supercapacitors due to its small area-normalized specific capacitance.[25] On the other hand, though it has also been practiced recently to make graphene-based composite electrodes using metal oxides and/or conductive polymers, the pseudo-capacitance usually suffered from inferior power performance and cyclicity.[26–32]

## Experimental section

Graphene oxide was synthesized from graphite by a modified Hummers method. Graphite and $NaNO_3$ were first mixed together in a flask. After that, $H_2SO_4$ (100 ml, 95%) was added to the flask which was kept in an ice bath while being stirred. Potassium permanganate (8 g) was added to the suspension slowly to avoid overheating. The mixture was then stirred at room temperature for 2 h. The colour of the suspension will become bright brown. Then, distilled water (90 ml) was added to the flask with stirring. The temperature of the suspension will quickly reach 90 °C and the colour would change to yellow. The diluted suspension was then stirred at 98 °C for 12 h. $H_2O_2$ (30 ml of 30%) was then added to the mixture. For purification, the mixture was washed by rinsing with 5% HCl and then deionized water several times. After that the suspension was centrifuged at 4000 rpm for 6 min. After filtration and drying in a vacuum, the graphene oxide was obtained as black powders.

100 mg graphene oxide powders were then dispersed into distilled water (30 ml) with sonication for 30 minutes. The suspension was subsequently heated on a hot plate to reach 100 °C and hydrazine hydrate (3 ml) was then added into the suspension. The suspension was kept at 98 °C for reduction for 24 h. After that the reduced graphene was collected by filtration as black powders. The obtained filtration pellet was then washed with distilled water several times to remove the excess hydrazine and redistribute into water by sonication. Then the suspension is centrifuged at 4000 rpm for 3 min to remove large graphite particles. The final graphene product was collected by vacuum filtration and dried in a vacuum.

Single-walled carbon nanotubes (SWCNTs) of high surface area (407 $m^2$ $g^{-1}$) and high conductivity (100 S $cm^{-1}$) were purchased commercially (Cheap Tube, Inc., purity >90%, amorphous carbon content <3 wt%, length 5–30 μm, diameter 1–2 nm). The carbon nanotubes were used without any further treatment.

The two electrodes were assembled with CNTs, graphene and graphene/CNT composite using the same mass of material. The SWCNTs and graphene were first dispersed separately in ethanol of concentration 0.2 mg $ml^{-1}$. Then the suspensions are filtered onto a microporous filter paper by vacuum filtration. The graphene/CNT composite film is prepared by mixing graphene and CNTs by sonication in ethanol followed by vacuum filtration. The films made of CNTs, graphene, and graphene/CNT composite were attached to a high purity titanium current collector in the test cell. The two electrodes were separated by a thin polypropylene film in 1 M KCl aqueous electrolyte solution, 1 M $TEABF_4$/PC organic electrolyte and 1-ethyl-3-methyl imidazolium bis(trifluoromethane sulfone) imide (EMI-TFSI).

The electrodes of CNTs, graphene and graphene/CNT were prepared by cutting the filtered CNTs, graphene and graphene/CNT film into 1 × 2 $cm^2$ with the weight of 1 mg. The graphene/CNT electrodes used in ionic liquid were assembled into a coin cell supercapacitor with 1.6 mg of each electrode in a glovebox.

The morphologies and structure of the CNTs, graphene, and graphene/CNT composite were examined by both scanning electron microscope (SEM, JSM-6500F) and transmission electron microscope (TEM, JEM-2100). The surface area and pore size distribution are measured with AUTOSORB-1 of Quantachrome Instruments.

## Results and discussion

In our experiment, chemically reduced graphene and CNTs were mixed with the aid of sonication. In order to make a uniform graphene/CNT composite film, it is crucial to produce a homogeneous graphene/CNT suspension. The graphene can also act as a surfactant to help disperse the carbon nanotubes in water. There have been several studies reporting CNTs as a water soluble material.[33,34] Most of the surfactants have polyaromatic components. However, these large molecular surfactants often bring some undesired effects to the carbon nanotubes. For example, the surfactant polymer would reduce the electrical conductivity of the CNTs.[35] On the other hand, graphene can assist the dispersion of CNTs in water. A chemically reduced graphene has many π-conjugated aromatic domains in its basal plane. Strong interactions with the surface of CNTs can take place through the π–π attractions.[36] Our graphene material has excellent water dispersibility. It can be seen in Fig. 2a, where the graphene disperses very well in water after 2 hours. In contrast, the single-walled carbon nanotube material does not disperse at all in distilled water. Therefore, the excellent water processability of the chemically

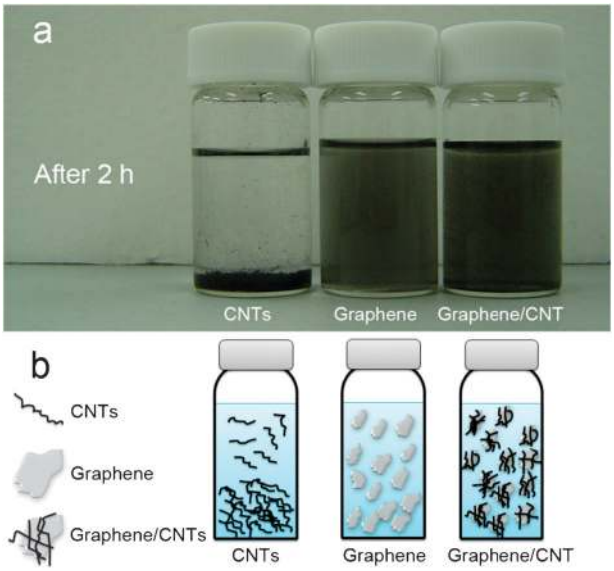


**Fig. 2** Interaction of chemically reduced graphene and CNTs in water. (a) Dispersibility of CNTs, graphene, and graphene/CNT composite in water for 2 hours after sonication. (b) Schematic illustration of the respective structures in suspension.

reduced graphene can help disperse the CNTs in water to form a homogenous solution. To make a thin film by vacuum filtration in our experiment, we need the CNTs to disperse well and be stable for 1 hour at least. Fig. 2b shows schematically the functions of graphene in assisting the dispersion of CNTs in the graphene/CNT composite. The single-walled carbon nanotubes used in our experiment are of 5–30 μm in length and they entangle with the graphene nano-sheets very easily. In this way, we obtained a homogenous graphene/CNT suspension and a uniform composite film.

Fig. 3 shows the morphologies of the CNTs, graphene, and the graphene/CNT composite electrode. Fig. 3a shows the conformal morphology of the graphene/CNT film, which is essential for achieving a high film conductivity. We can see that the CNTs are very long and they entangled with each other like a spider web. This kind of web-like structure can trap the graphene nano-sheets or other structures that are in contact with them. We can also see some amorphous carbon attached on the film. Fig. 3b and c are SEM images of the graphene/CNT composite at different magnifications, revealing the blending of the graphene nano-sheets and CNTs. Since the CNTs have highest electrical conductivity, this structure is suggested to reduce the electrical resistance of the electrode, because the CNTs can act as the "pathways" for the ions and electrons. In addition, the CNTs can also act as a spacer of the graphene nano-sheets, which would then enhance the ion accessibility. Fig. 3d is a TEM image of the carbon nanotubes. Some of CNTs were entangled into bundles. The inset is an electron diffraction pattern of the CNTs. Fig. 3e is a TEM image of a typical structure of graphene nano-sheet, indicating that graphite has been extensively exfoliated to produce monolayer and few-layer graphene. In fact, we also found that some sediment had not been exfoliated by the chemical method. A more definitive identification of graphene can be made by an analysis of the electron diffraction patterns. The inset of Fig. 3e is an example of this. This diffraction pattern is acquired at the red spot indicated in Fig. 3e, and it has the typical six-fold symmetry expected for graphite or graphene. The {110}* reflections are more intensive than the {100}* reflections, indicating that it is a multilayer graphene.[37] Fig. 3f is a TEM image of the graphene/CNT composite. The CNTs were entangled into bundles, and some small pieces of graphene (indicated by arrows) nano-sheets were also seen to have been attached on the CNT bundles.

The capacitance of a supercapacitor is strongly dependent on the cell configuration used for the electrochemical measurement and it is always significantly higher when using a three-electrode system.[38] A two-electrode test cell was used in this work because it can provide the most accurate measurement of the material performance for the supercapacitor.[39] The two electrodes were assembled without using any binder in our experiment. The supercapacitors were tested with two different electrolytes that are used routinely for the electrochemical double-layer capacitors. The aqueous electrolyte is 1 M KCl, and the

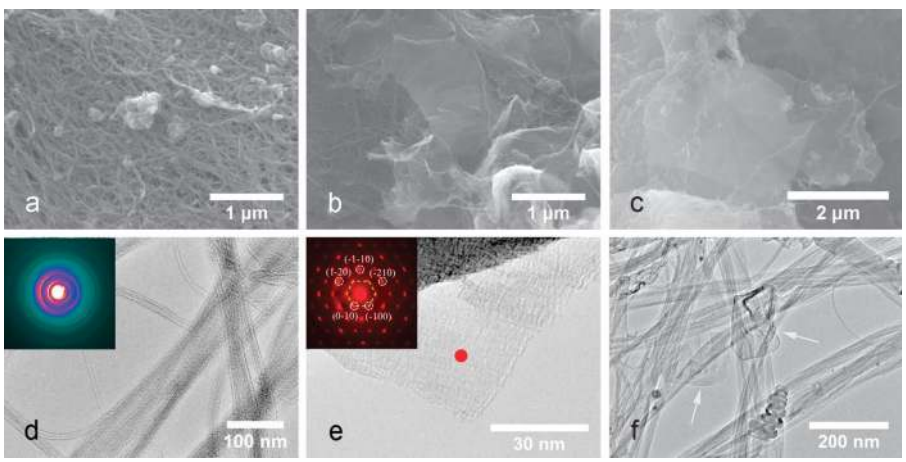


**Fig. 3** Morphological and structural characterization of various carbon electrodes. (a) SEM image of the CNT film. (b) SEM image of the graphene/CNT composite at low magnification. (c) SEM image of the graphene/CNT composite at high magnification. (d) TEM image of CNTs. Inset is an electron diffraction pattern. (e) TEM image of the prepared graphene. Inset is an electron diffraction pattern acquired at the location indicated in the image. (f) TEM image of the graphene/CNT composite.

 

organic electrolyte is 1 M tetraethylammonium tetrafluoroborate ($TEABF_4$) in propylene carbonate (PC). The electrochemical properties and capacitance of the supercapacitor electrodes were measured using the two-electrode system by cyclic voltammetry (CV), galvanostatic charge/discharge, and electrochemical impedance spectroscopy (EIS). The galvanostatic charge/discharge was used to obtain the specific capacitance of the three different types of electrodes. Impedance spectroscopy measurement was carried out without the sinusoidal DC bias of 0.005 V in the frequency window from 0.1 Hz to 100 kHz. Fig. 4 shows the electrochemical measurement of pristine CNTs, pristine graphene, and graphene/CNT composite electrodes. Fig. 4a and b are the CV curves in aqueous and organic electrolytes at the scan rate of 10 mV $s^{-1}$, respectively. The graphene/CNT composite showed the largest current in both aqueous and organic electrolytes, indicating the largest specific capacitance. It is worth noting that the CV curves shown in Fig. 4a have the most rectangular geometry, indicating excellent charge propagation in the electrodes. The shape of the CV loop of a supercapacitor should be rectangular provided that there is a low contact resistance. Larger resistance distorts the loop, resulting in a narrower loop with an oblique angle. It can be observed from Fig. 4b that the CV curve in the organic electrolyte does not exhibit rectangular geometry due to the larger resistance in the organic electrolyte. Water content and redox groups such as hydroxide group and carboxyl may also cause the irregular shape of the CV curve. Fig. 4c and d are the galvanostatic charge/discharge curves in the two types of electrolytes. We can see from Fig. 4c and d that the CNTs produce the most symmetric charge/discharge curve, indicating the smallest resistance. But the CNTs have the smallest specific capacitance that is calculated from the galvanostatic charge/discharge curve. Meanwhile, the graphene/CNT composite electrode has the largest specific capacitance and a smaller resistance than pristine graphene. This indicates that the graphene/CNT composite can enhance both the energy (related to specific capacitance) and power (related to resistance) performance. The outstanding electrochemical properties of the graphene/CNT composite are attributed to the nanoscale structure of graphene and CNTs. This structure brings several advantages to its functions: firstly, the highly conductive CNTs can provide a pathway for the transportation of ions and electrons, which in turn reduces the internal resistance; secondly, the carbon nanotubes with a length of about 30 μm are likely to entangle with each other, as shown in Fig. 3a, to make the CNTs act as an effective conductive binder to hold the graphene nano-sheets; thirdly, the entangled CNTs on the surface of graphene nano-sheets can also act as a spacer that prevents the graphene nano-sheets from agglomerating, resulting in an enhanced ion exchange rate.

Fig. 5a shows the CV curves of the graphene/CNT composite electrode in the aqueous and organic electrolytes, respectively. The composite electrode shows a more rectangular CV curve in the aqueous electrolyte at a high scan rate of 100 mV $s^{-1}$, indicating very good charge propagation within the electrode. The deviation of the CV curves in the organic electrolyte is attributed to poor conductivity of the electrolyte and water content. Fig. 5b is a comparison of the galvanostatic

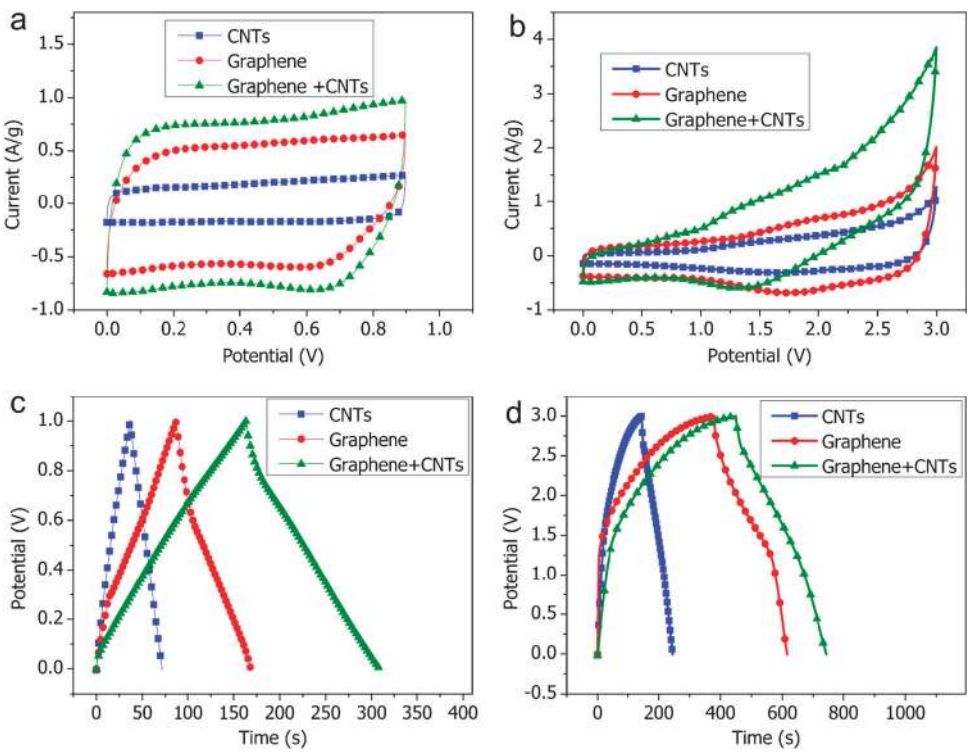


**Fig. 4** Electrochemical properties of various electrodes made of CNTs, graphene, and graphene/CNT composite. (a) Cyclic voltammetry curves in the aqueous electrolyte at a scan rate of 10 mV $s^{-1}$. (b) Cyclic voltammetry curves in 1 M $TEABF_4$/PC electrolyte at the same scan rate of 10 mV $s^{-1}$. (c) Galvanostatic charge/discharge curves in the aqueous electrolyte at a charging current of 500 mA $g^{-1}$. (d) Galvanostatic charge/discharge curves in the organic electrolyte at the same charging current of 500 mA $g^{-1}$.

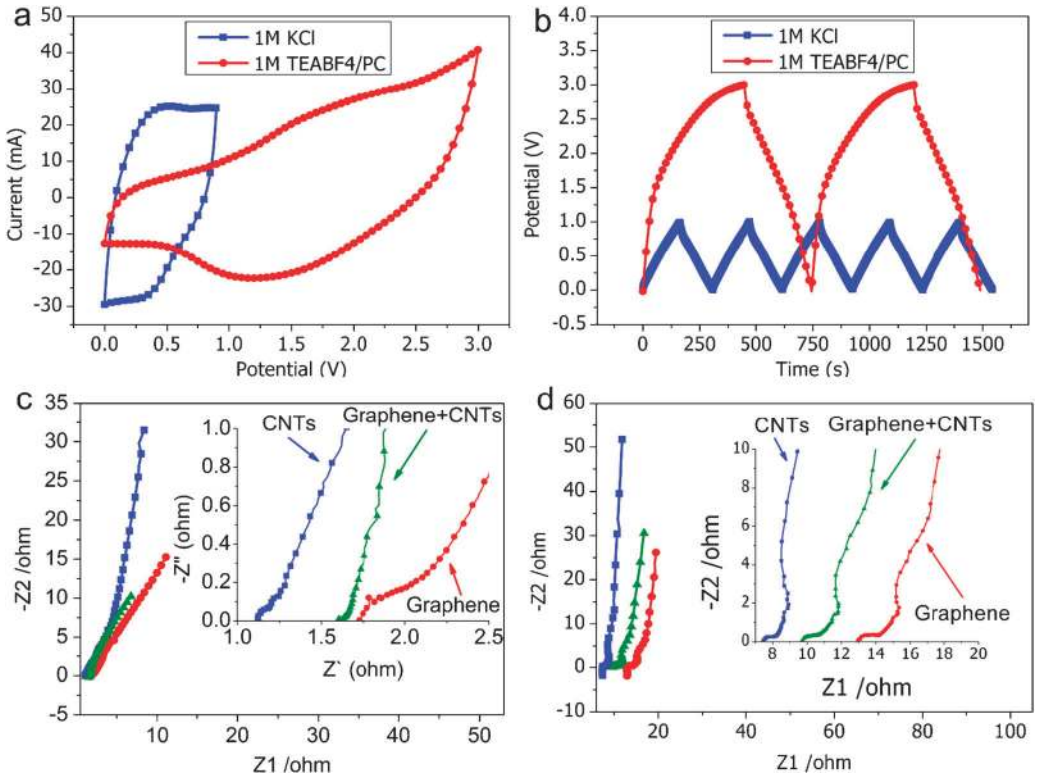


**Fig. 5** Comparison of electrochemical behaviors of the studied electrodes made of CNTs, graphene, and graphene/CNT composite. (a) Comparison of the graphene/CNT composite electrode in aqueous and organic electrolytes at a scan rate of 100 mV $s^{-1}$. (b) Comparison of galvanostatic charge/discharge curves of the graphene/CNT composite in aqueous and organic electrolytes at a charging current of 0.5 A $g^{-1}$. (c) EIS test of CNTs, graphene, and graphene/CNT composite in the KCl electrolyte. (d) EIS measurement of CNTs, graphene, and graphene/CNT composite in the $TEABF_4$/PC electrolyte.

charge/discharge curves in the two different electrolytes at the same charge current density of 0.5 A $g^{-1}$. It is worth mentioning that the specific capacitance is strongly dependent on the measurement system of the supercapacitor. The three electrode system always has a significantly higher testing value than the two electrode system which has more accurate data. In our experiment, symmetrical electrodes were used for the supercapacitor testing with the same weight. The specific capacitance for the whole cell (two electrodes) is 72.6 F $g^{-1}$ in the aqueous electrolyte and 50.3 F $g^{-1}$ in the organic electrolyte. The specific capacitance of each electrode (single electrode) can also be calculated according to eqn (1) and (2) given below, which is four times the total cell specific capacitance.

$$\frac{1}{C_{\text{total}}} = \frac{1}{C} + \frac{1}{C} \quad (1)$$

$$\frac{C^{\text{s}}}{C^{\text{s}}_{\text{total}}} = \frac{C/m}{C_{\text{total}}/2m} = \frac{4}{1} \quad (2)$$

In the above equations, $C_{\text{total}}$ is the total capacitance of the testing cell, $C^{\text{s}}$ is the specific capacitance of each electrode, $C^{\text{s}}_{\text{total}}$ is the specific capacitance of the whole testing cell, and $m$ is the mass of each electrode. Therefore the specific capacitance for each electrode of our cell is 290.4 F $g^{-1}$ in the aqueous electrolyte and 201.0 F $g^{-1}$ in the organic electrolyte, respectively.

Fig. 5c and d show the Nyquist plots in the two electrolytes. In the complex plane, the imaginary component, Z2, shows the capacitive property and the real component, Z1, shows the ohmic property. Both components have been studied in the frequency range between 0.1 Hz and 100 000 Hz. These plots usually consist of one or more semicircles in the complex plane, sometimes with the centre of a semicircle depressed below the Z1 axis. The theoretical Nyquist plot of a supercapacitor consists of three regions which are dependent on the frequencies. At very high frequency, the supercapacitor behaves like a pristine resistor. At low frequency, the imaginary part sharply increases and a nearly vertical line is observed, indicating a pristine capacitive behaviour. In the medium frequency domain, the influence of the electrode porosity can be observed. When the frequency decreases, starting from the very high frequency, the signal penetrates deeper and deeper into the porous structure of the electrode, then more and more electrode surface becomes available for ion adsorption. This medium frequency range is related to the electrolyte penetration in the porous structure of the high porosity electrode and this region is usually called the Warburg curve.[40] Fig. 5c and d are the EIS of CNTs, graphene, and graphene/CNT composite in the aqueous electrolyte and in the organic electrolyte, respectively. All the EIS lines show a linear behaviour in the low frequency region and an arc in the high frequency region. The loop shifts near the high frequency region are related to the electrical resistance between the graphene nano-sheets. The semicircle region has been observed in all carbon-based supercapacitors. It usually exhibits a very large semicircle in the activated carbon

 

electrode supercapacitor which means a large inter-granular electrical resistance between the activated carbon particles. It mainly depends on the electrode surface area and the inter-particle resistance. The formation of thin active layers or addition of conductive additives with low surface area can reduce this value, but they will lead to a low capacitance per area or capacitance per weight. The extremely small semicircular regions in Fig. 5c and d show a low electrical resistance between the graphene nano-sheets and good conductance between the graphene electrode and the current collector. We can therefore observe from the EIS curves in the two electrolytes that the semicircular region for the graphene/CNT composite is smaller than that for pristine graphene, indicating that the additions of CNTs reduced the interlayer resistance of the graphene sheets and the contact resistance with the current collector. The Warburg curves which are known to be a straight line that is at a 45° angle from the lower left to the upper right in the Nyquist plot in Fig. 5c and d are very short, indicating an enhanced access of electrolytic ions to the graphene surface in both electrolytes. The equivalent series resistance (ESR) is obtained from the $x$-intercept of the Nyquist plot. They are 1.1 Ω (CNTs), 1.68 Ω (graphene), 1.6 Ω (graphene/CNT) in the aqueous electrolyte, and 7.8 Ω (CNTs), 12.9 Ω (graphene), 9.73 Ω (graphene/CNT) in the organic electrolyte, respectively. The ESR data determine the rate at which the supercapacitor can be charged and discharged, and it is a very important factor to determine the power density of a supercapacitor since the power density is inversely proportional to ESR. A summary of the electrochemical properties is given in Fig. 6, from which we can see that the graphene/CNT composite has the highest power and energy performance. The energy density and power density are calculated according to eqn (3) and (4):

$$E_{\text{density}} = \tfrac{1}{2} C_{\text{sp}} V^2 \tag{3}$$

and

$$P_{\text{density}} = \frac{V^2}{4mR_{\text{esr}}}, \tag{4}$$

where $E_{\text{density}}$ and $P_{\text{density}}$ stand for energy density and power density, respectively, $C_{\text{sp}}$ is the specific capacitance, $R_{\text{esr}}$ is the equivalent series resistance, $m$ is the total weight of the two electrodes, and $V$ is the maximum charging voltage. We used 1 V for the aqueous electrolyte, 3 V for the organic electrolyte in our experiments and calculations.

Rate capability is also important for evaluating the performance of a supercapacitor. A good energy storage device is required to provide its energy through a high current. Fig. 7 shows the specific capacitance of CNTs, graphene, and graphene/CNT composite electrode at different charging current densities. We obtained the largest specific capacitance of 290.4 F $g^{-1}$ in 1 M KCl electrolyte and 201.0 F $g^{-1}$ in 1 M $TEABF_4$ electrolyte at the charging current of 0.5 A $g^{-1}$ for a single electrode. We obtained 217.0 F $g^{-1}$ in 1 M KCl electrolyte and 150.8 F $g^{-1}$ in 1 M $TEABF_4$ electrolyte at the charging current of 2 A $g^{-1}$ for a single electrode. This means that the graphene/CNT composite electrode preserved 75% of specific capacitance in both the aqueous electrolyte and the organic electrolyte when the charging current increased from 0.5 A $g^{-1}$ to 2 A $g^{-1}$. It has a better performance than the pristine graphene electrode

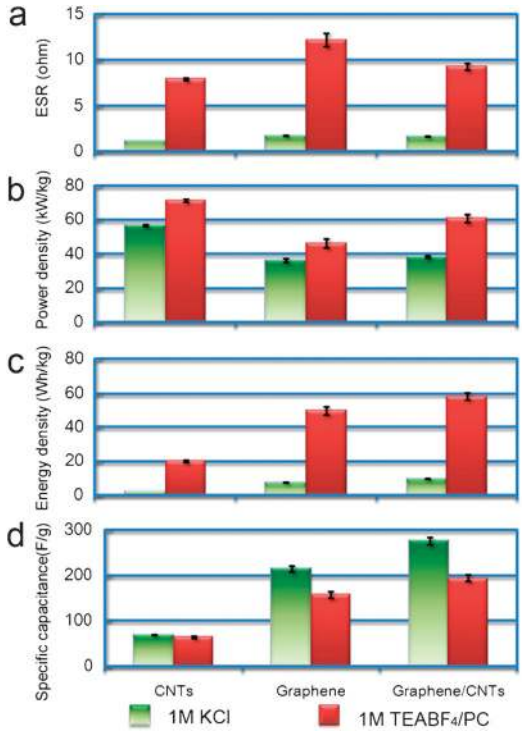


**Fig. 6** Summary of electrochemical properties of CNTs, graphene, and graphene/CNT composite electrodes. (a) Equivalent series resistance (ESR) of CNTs, graphene, and graphene/CNT composite in both the aqueous electrolyte and the organic electrolyte. (b) Comparison of power densities. (c) Comparison of energy densities. (d) Comparison of specific capacitance.

which preserved about 65% in the electrolytes as the charging current increased from 0.5 A $g^{-1}$ to 2 A $g^{-1}$. The pristine CNT electrode preserved almost 93% in both electrolytes when the

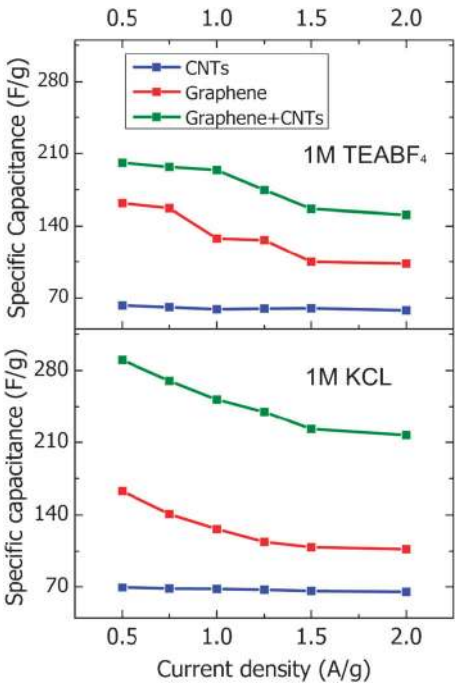


**Fig. 7** Specific capacitance of CNTs, graphene, graphene/CNT composite supercapacitors at different charging current densities.

charging current changed. This performance is explained as follows. The CNT film has large pores accessible for the electrolyte ions. A high charging current means a higher rate of ion exchange. Pristine graphene does not have a good rate capability because of the aggregation after drying, which usually leads to an ultra-small pore size. At a high charging rate, the electrolyte ions do not have enough time to enter the ultra-small pores and it results in a smaller specific capacitance at high charging current. Therefore, we believe that the graphene/CNT composite has a higher rate capability than pristine graphene because the graphene sheets are intertwined with CNTs resulting in larger spaces between each sheets and a larger pore size as well.

The graphene/CNT composite electrode shows good energy performance in the organic electrolyte. However, the energy density of 62.8 Wh $kg^{-1}$ still needs to be improved for portable electronics and vehicle applications. Therefore we should note from eqn (3) that the energy density is in proportion to power squared of the charging voltage. We expect our graphene/CNT electrodes to produce an even higher energy density at room temperature in ionic liquid of 1-ethyl-3-methyl imidazolium bis(trifluoromethane sulfone)imide (EMI-TFSI) with a charging voltage of 4 V. Ionic liquids, which exhibit high ionic conductivity, large electrochemical windows (up to 7 V), excellent thermal stability (−40 to +200 °C typical), and characteristics of being nonvolatile, nonflammable, and non-toxic, are very suitable for supercapacitors for achieving high energy density applications, such as electric vehicles. Two pieces of electrodes with a mass of 1.6 mg each were also assembled into a coin-cell supercapacitor in a glovebox in our experiment. The CV curves of the graphene/CNT electrodes are given in Fig. 8a. Oblique CV curves are observed because of the relatively larger resistance of the electrolyte and the contact between electrodes and electrolyte than that of the aqueous electrolyte. No oxidation or reduction peaks were noticed in the CV curves. We also evaluated the rate capability of graphene/CNT electrodes in EMI-TFSI, which is shown in Fig. 8b. The specific capacitance reached 280 F $g^{-1}$ at a current density of 0.3 A $g^{-1}$. We could have a specific capacitance of 161.9 F $g^{-1}$ at a very large current density of 3.1 A $g^{-1}$. The graphene/CNT composite preserved 68% in an ionic liquid electrolyte when the current density increased from 0.3 to 2.0 A $g^{-1}$.

Life time and durability are also important for evaluating an energy storage system. To address this issue we performed 1300 complete charging and discharging cycles at 2 A $g^{-1}$ from 0 to 1 V for the aqueous electrolyte and 4 V for ionic liquid. We also studied the pristine graphene and SWCNTs under the same experimental conditions in the aqueous electrolyte for comparison (Fig. 9a). The SWCNTs declined by 9.3% after 1300 cycles. However, there is a very interesting phenomenon that the specific capacitance of graphene and graphene/CNTs did not decrease in the 1300 cycles in 1 M KCl but actually having increased dramatically. We named this phenomenon as "electro-activation".[13] The same phenomenon was also observed in the ionic liquid electrolyte. A representative long-time cycling of the graphene/CNT electrode in EMI-TFSI is shown in Fig. 9b. The specific capacitance increased by 29% after 1000 cycles in the ionic liquid electrolyte suggesting an excellent cyclicity. This "electro-activation" is suggested to occur because the graphene sheets would move to adjust to different electrolyte ions. The long time charging and discharging should also help the ions accessing the graphene sheets to take advantages of the large surface area of graphene. For the few-layered graphene sheets, they are more likely to aggregate to form thicker layers (Fig. 10a). The long time cycling should help ions intercalate into the space of the graphene sheets and therefore lead to a larger spacing between the layers, which would in turn provide an even larger surface area available for the "double-layer" capacitance (Fig. 10b). This is why we have observed that the specific capacitance actually increased during cycling. The specific capacitance of the pristine graphene electrode increased by 60% after the long time cycling while that of the graphene/CNT composite electrode increased by 18% after the cycling in the aqueous electrolyte and specific capacitance increased by 29% in ionic liquid.

The graphene/CNT electrode used in ionic liquid showed outstanding energy performance of 155.6 Wh $kg^{-1}$ and it is much better than commercial products.[41] The improvement is attributed to a higher accessible specific surface area and higher efficiency of electrolytic ion absorption. In the graphene/CNT composite, individual single-layered or few layered graphene nano-sheets offer an ideal structure for ion absorption. Moreover, the graphene-based electrode does not depend on the exact pore distribution in the solid support to provide a large surface area. A graphene nano-sheet can adjust itself to the different types of electrolytes. Thus, access to the very high surface area of graphene material by the electrolyte can be maintained while preserving an overall high electrical conductivity. The graphene/CNT electrode can also have

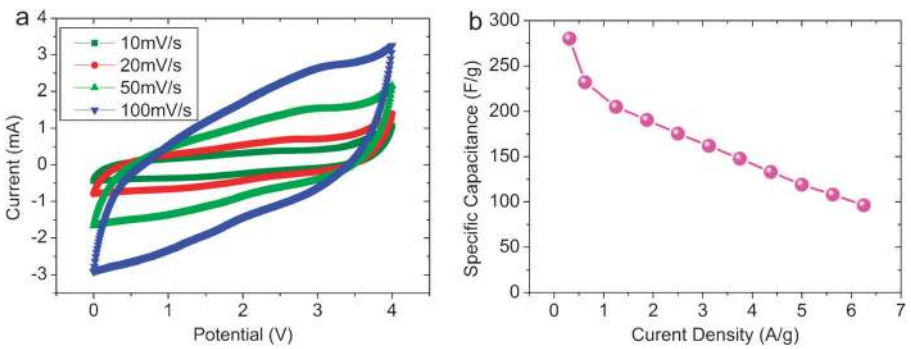


**Fig. 8** (a) Cyclic voltammetry curves in ionic liquid at scan rates of 10, 20, 50, and 100 mV $s^{-1}$. (b) Specific capacitance of graphene/CNT composite supercapacitors in an ionic liquid electrolyte at different charging current densities.

 

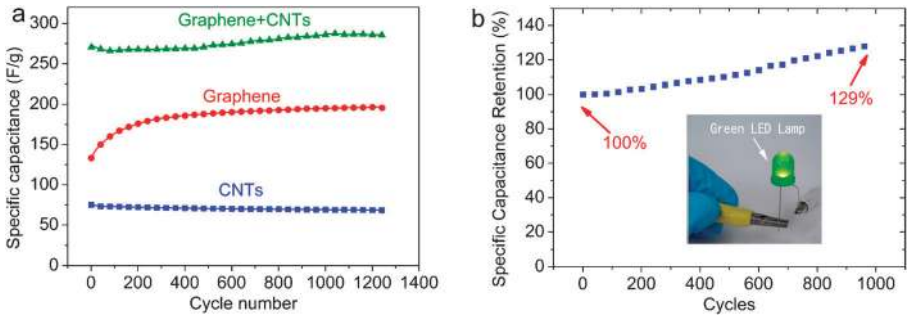


**Fig. 9** (a) Cycling property of SWCNTs, graphene, and graphene/CNT composite electrodes in 1 M KCl. (b) Cycling performance of the graphene/CNT composite electrode in EMI-TFSI. The inset is a full cell with graphene/CNT electrodes to light up LEDs.

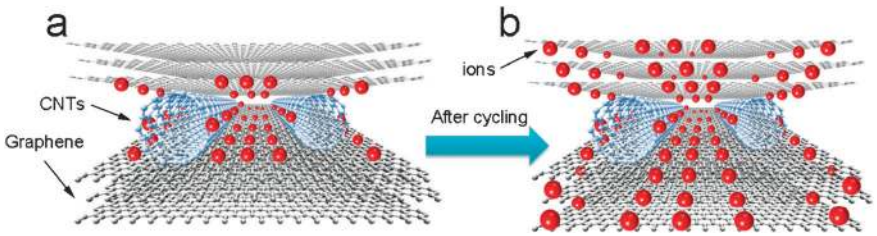


**Fig. 10** Schematic illustrating the electro-activation to increase the electrode surface area after cycling. (a) Graphene sheets are likely to aggregate to form few-layered graphene which cannot be fully accessed by electrolyte ions at the first several charging and discharging cycles. (b) After long time cycling, aggregated graphene sheets are separated by intercalated ions. So there is more and more surface area available for electrolyte ions to result in an increase of specific capacitance after cycling.

a larger thickness than the activated carbon based electrode, resulting in an even higher capacitance per area. This is because activated carbon has larger electrical resistance which limits its thickness and usually contains conductive but low surface area additives such as carbon blacks to enable a rapid electrical charge transfer from the cell.[8] The high electrical conductivity of the graphene/CNT composite eliminates the need for conductive fillers and allows increased electrode thickness. Increasing the electrode thickness and elimination of additives lead to an improved collector/separator ratio, which in turn further increases the energy density of the supercapacitor. The addition of CNTs can increase the conductivity of the electrode, which can then increase the power density of the electrode. Moreover, the graphene/CNT electrodes can reach a maximum power density of 263.2 kW $kg^{-1}$.

An understanding of the surface area and porosity of the graphene/CNT composite can be achieved by the adsorption and desorption isotherm given in Fig. 11. The specific surface area of the graphene/CNT composite is 421.3 $m^2$ $g^{-1}$ measured by the multipoint Brunauer–Emmett–Teller (BET) method. The nitrogen adsorption isotherm of the graphene/CNT composite shows a type IV isotherm characterized by hysteresis between the adsorption and desorption isotherms and the steep slope at higher relative pressures, which is associated with mesoporosity. Moreover, the mixed type A and B hysteresis loops are associated with tubular capillaries open at both ends and the space between parallel plates, which are attributed to the unique structure of the graphene/CNT composite.[42] The increase of specific capacitance of our graphene/CNT composite electrodes compared to pristine graphene electrodes in the aqueous electrolyte and the excellent performance in ionic liquid of graphene/CNT composite are attributed to the increased average pore size as shown in the

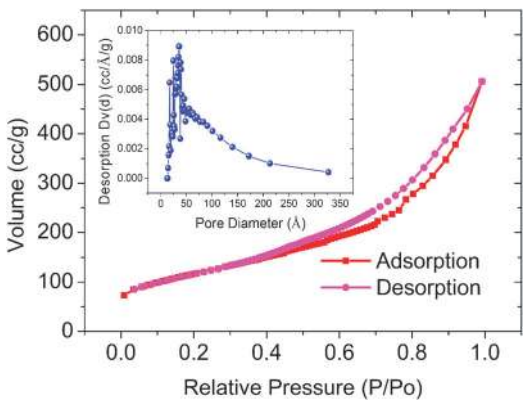


**Fig. 11** Nitrogen adsorption isotherm of the graphene/CNT composite. The inset graph is the pore size distribution of the graphene/CNT composite.

inset of Fig. 11, which is calculated by the Barrett, Joyner and Halenda (BJH) method. The graphene/CNT composite has pores of sizes between 1.3 nm to 32.7 nm with an average pore size of 6.1 nm. The average pore size of the pristine graphene is 3.2 nm. This suggests that the SWCNTs act as a smart spacer to increase the pore size and contribute to better electrolyte accessibility and rate capability.

To demonstrate a practical supercapacitor, a coin cell supercapacitor using our graphene/CNT electrodes in both the cathode and anode was also assembled to light up a green light-emitting diode (LED) lamp alternately as shown in Fig. 9b. The graphene/CNT composite electrode-based supercapacitor has a comparable energy density to the nickel metal hydride (NiMH) battery with an energy density of 30–100 Wh $kg^{-1}$

but has a much better power performance than the NiMH battery (0.25–1 kW $kg^{-1}$) that is now used widely in hybrid vehicles such as Toyota Prius and Honda Insight. The NiMH batteries are limited by their service life, discharge current, self-discharge, and poor temperature adaption.[43] The graphene-based supercapacitors can overcome these problems without losing their performance. In this regard, the supercapacitors made of graphene/CNT electrodes with smart device packing are showing great promising potentials for uses in electric energy storage for hybrid vehicles.

In our experiment, we found that pristine graphene could not be used without any binder. We soaked the pristine graphene electrodes in 1 M KCl for 3 days and lost about 45% of weight after soaking. For SWCNT electrodes, we reserved almost 100% after 3 day soaking. This is because SWCNTs entangled with each other and do not need any binder to hold them together. Therefore we believe that the SWCNTs can be used as a binder for the graphene/CNT composite electrodes. When we put the graphene/CNT composite electrode into the electrolyte for the same period of time, we found that 95% was reserved, indicating excellent stability of the graphene/CNT composite electrodes.

## Conclusions

In summary, we have successfully fabricated high performance graphene/CNT supercapacitors with a specific capacitance of 290.4 F $g^{-1}$ measured with a more practical two-electrode system. We obtained an energy density of 62.8 Wh $kg^{-1}$ and a power density of 58.5 kW $kg^{-1}$, which are 23% and 31% higher than using a pristine graphene electrode in an organic electrolyte, respectively. Moreover we estimated that our composite electrodes in ionic liquid would produce an energy density of 155.6 Wh $kg^{-1}$ and a maximum power density of 263.2 kW $kg^{-1}$. The high energy and power performance makes the supercapacitors a promising candidate for use in hybrid vehicles and electrical vehicles. Furthermore, the results are also potentially useful for preparation of other graphene-based composite films in order to meet diverse application requirements, such as lithium ion batteries, electrochemical sensors, and solar cells.

## Acknowledgements

This work was supported by JSPS Grants-in-Aid for Scientific Research No. 19310081 and 22310074, and the Nanotechnology Network Project of the Ministry of Education, Culture, Sports, Science and Technology (MEXT), Japan.

## References

1 L. L. Zhang and X. S. Zhao, *Chem. Soc. Rev.*, 2009, **38**, 2520–2531.
2 J. R. Miller and P. Simon, *Science*, 2008, **321**, 651–652.
3 E. Frackowiak and F. Beguin, *Carbon*, 2001, **39**, 937–950.
4 E. Frackowiak and F. Beguin, *Carbon*, 2002, **40**, 1775–1787.
5 D. N. Futaba, K. Hata, T. Yamada, T. Hiraoka, Y. Hayamizu, Y. Kakudate, O. Tanaike, H. Hatori, M. Yumura and S. Iijima, *Nat. Mater.*, 2006, **5**, 987–994.
6 A. Izadi-Najafabadi, S. Yasuda, K. Kobashi, T. Yamada, D. N. Futaba, H. Hatori, M. Yumura, S. Iijima and K. Hata, *Adv. Mater*, 2010, **22**, E235–E241.
7 Y. Wang, Z. Q. Shi, Y. Huang, Y. F. Ma, C. Y. Wang, M. M. Chen and Y. S. Chen, *J. Phys. Chem. C*, 2009, **113**, 13103–13107.
8 M. D. Stoller, S. J. Park, Y. W. Zhu, J. H. An and R. S. Ruoff, *Nano Lett.*, 2008, **8**, 3498–3502.
9 D. W. Wang, F. Li, J. P. Zhao, W. C. Ren, Z. G. Chen, J. Tan, Z. S. Wu, I. Gentle, G. Q. Lu and H. M. Cheng, *ACS Nano.*, 2009, **3**, 1745–1752.
10 Y. Q. Sun, Q. O. Wu and G. Q. Shi, *Energy Environ. Sci.*, 2011, **4**, 1113–1132.
11 M. Pumera, *Energy Environ. Sci.*, 2011, **4**, 668–674.
12 C. Peng, S. W. Zhang, X. H. Zhou and G. Z. Chen, *Energy Environ. Sci.*, 2010, **3**, 1499–1502.
13 Q. Cheng, J. Tang, J. Ma, H. Zhang, N. Shinya and L. C. Qin, *Carbon*, 2011, **49**, 2917–2925.
14 J. C. Meyer, A. K. Geim, M. I. Katsnelson, K. S. Novoselov, T. J. Booth and S. Roth, *Nature*, 2007, **446**, 60–63.
15 C. Gomez-Navarro, R. T. Weitz, A. M. Bittner, M. Scolari, A. Mews, M. Burghard and K. Kern, *Nano Lett.*, 2007, **7**, 3499–3503.
16 H. A. Becerril, J. Mao, Z. Liu, R. M. Stoltenberg, Z. Bao and Y. Chen, *ACS Nano*, 2008, **2**, 463–470.
17 A. G. Pandolfo and A. F. Hollenkamp, *J. Power Sources*, 2006, **157**, 11–27.
18 V. C. Tung, M. J. Allen, Y. Yang and R. B. Kaner, *Nat. Nanotechnol.*, 2009, **4**, 25–29.
19 S. Stankovich, D. A. Dikin, G. H. B. Dommett, K. M. Kohlhaas, E. J. Zimney, E. A. Stach, R. D. Piner, S. T. Nguyen and R. S. Ruoff, *Nature*, 2006, **442**, 282–286.
20 A. K. Geim and P. Kim, *Sci. Am.*, 2008, **298**, 90–97.
21 J. Yan, T. Wei, B. Shao, F. Q. Ma, Z. J. Fan, M. L. Zhang, C. Zheng, Y. C. Shang, W. Z. Qian and F. Wei, *Carbon*, 2010, **48**, 1731–1737.
22 C. G. Liu, Z. N. Yu, D. Neff, A. Zhamu and B. Z. Jang, *Nano Lett.*, 2010, **10**, 4863–4868.
23 D. S. Yu and L. M. Dai, *J. Phys. Chem. Lett.*, 2010, **1**, 467–470.
24 Z. J. Fan, J. Yan, L. J. Zhi, Q. Zhang, T. Wei, J. Feng, M. L. Zhang, W. Z. Qian and F. Wei, *Adv. Mater.*, 2010, **22**, 3723–3728.
25 V. C. Tung, L. M. Chen, M. J. Allen, J. K. Wassei, K. Nelson, R. B. Kaner and Y. Yang, *Nano Lett.*, 2009, **9**, 1949–1955.
26 L. L. Zhang, S. Y. Zhao, X. N. Tian and X. S. Zhao, *Langmuir*, 2010, **26**, 17624–17628.
27 Z. S. Wu, D. W. Wang, W. Ren, J. Zhao, G. Zhou, F. Li and H. M. Cheng, *Adv. Funct. Mater.*, 2010, **20**, 3595–3602.
28 H. L. Wang, Q. L. Hao, X. J. Yang, L. D. Lu and X. Wang, *Nanoscale*, 2010, **2**, 2164–2170.
29 S. Biswas and L. T. Drzal, *Chem. Mater.*, 2010, **22**, 5667–5671.
30 J. Yan, T. Wei, W. M. Qiao, B. Shao, Q. K. Zhao, L. J. Zhang and Z. J. Fan, *Electrochim. Acta*, 2010, **55**, 6973–6978.
31 B. Wang, J. Park, C. Y. Wang, H. Ahn and G. X. Wang, *Electrochim. Acta*, 2010, **55**, 6812–6817.
32 J. Yan, T. Wei, Z. J. Fan, W. Z. Qian, M. L. Zhang, X. D. Shen and F. Wei, *J. Power Sources*, 2010, **195**, 3041–3045.
33 M. F. Islam, E. Rojas, D. M. Bergey, A. T. Johnson and A. G. Yodh, *Nano Lett.*, 2003, **3**, 269–273.
34 V. C. Moore, M. S. Strano, E. H. Haroz, R. H. Hauge, R. E. Smalley, J. Schmidt and Y. Talmon, *Nano Lett.*, 2003, **3**, 1379–1382.
35 J. Kang, S. Hong, Y. Kim and S. Baik, *Langmuir*, 2009, **25**, 12471–12474.
36 J. Kim, L. J. Cote, F. Kim, W. Yuan, K. R. Shull and J. X. Huang, *J. Am. Chem. Soc.*, 2010, **132**, 8180–8186.
37 Y. Hernandez, V. Nicolosi, M. Lotya, F. M. Blighe, Z. Y. Sun, S. De, I. T. McGovern, B. Holland, M. Byrne, Y. K. Gun'ko, J. J. Boland, P. Niraj, G. Duesberg, S. Krishnamurthy, R. Goodhue, J. Hutchison, V. Scardaci, A. C. Ferrari and J. N. Coleman, *Nat. Nanotechnol.*, 2008, **3**, 563–568.
38 E. Frackowiak, V. Khomenko, K. Jurewicz, K. Lota and F. Beguin, *J. Power Sources*, 2006, **153**, 413–418.
39 V. Khomenko, E. Frackowiak and F. Beguin, *Electrochim. Acta*, 2005, **50**, 2499–2506.
40 C. Portet, P. L. Taberna, P. Simon and C. Laberty-Robert, *Electrochim. Acta*, 2004, **49**, 905–912.
41 V. L. Pushparaj, M. M. Shaijumon, A. Kumar, S. Murugesan, L. Ci, R. Vajtai, R. J. Linhardt, O. Nalamasu and P. M. Ajayan, *Proc. Natl. Acad. Sci. U. S. A.*, 2007, **104**, 13574–13577.
42 B. Frisch and W. R. Thiele, *Powder Metall. Int.*, 1986, **18**, 17–21.
43 M. A. Fetcenko, S. R. Ovshinsky, B. Reichman, K. Young, C. Fierro, J. Koch, A. Zallen, W. Mays and T. Ouchi, *J. Power Sources*, 2007, **165**, 544–551.